Journal of Applied Polymer Science

Aluminum Silicate Fibers Impregnated Acrylonitrile Butadiene Rubber Composites: Ablation, Thermal Transport/Stability, and Mechanical Inspection

Nadeem Iqbal,[1] Sadia Sagar,[1] Mohammad Bilal Khan,[2] Mohamed Ismail Bassyouni,[3,4] Zaffar M. Khan[2]

[1]School of Chemical and Materials Engineering (SCME), NUST, Islamabad, Pakistan

[2]Centre for Energy Systems (CES), NUST, Islamabad, Pakistan

[3]Department of Chemical and Materials Engineering, College of Engineering Rabigh Campus, King Abdul-Aziz University, Kingdom of Saudi Arabia

[4]Department of Chemical Engineering, Higher Technological Institute, Tenth of Ramdan City, Egypt

Correspondence to: Nadeem Iqbal (E-mail: nadeemiqbal@scme.nust.edu.pk)

ABSTRACT: Variant concentrations of ceramic fibers (CerFs) were incorporated into acrylonitrile butadiene rubber (NBR) to fabricate elastomeric ablative composites for ultrahigh temperature applications. The CerFs introduction into the polymer matrix has enhanced the ablation resistance up to 59% and successfully reduced the backface temperature of the polymer composite up to 110°C during the ultrahigh temperature ablation investigation. Thermal decomposition of the polymer composites was diminished up to 10% with increasing fiber concentration in the rubber matrix. Thermal conductivity was reduced equal to 63% while thermal impedance was enhanced up to 84% with the utmost fiber incorporation into the NBR matrix. The CerFs have adversely affected the mechanical properties of NBR matrix due to their brittle/inert nature and weak interface bonding with the host matrix. Scanning electron microscopy along with the energy dispersive x-ray spectroscopy was used to examine the ablated specimens and the fiber dispersion within the host matrix. © 2013 Wiley Periodicals, Inc. J. Appl. Polym. Sci. 130: 4392–4400, 2013

KEYWORDS: composites; degradation; fibers; acrylonitrile butadiene; rubber; thermogravimetric analysis

Received 10 April 2013; accepted 30 June 2013; Published online 20 July 2013

DOI: 10.1002/app.39717

INTRODUCTION

Silica/silicon carbide fibers, carbon–carbon composites, phenolic composites, and elastomeric composite tiles have been used to protect reentry vehicles and solid rocket motor from ultrahigh temperature environments.[1–4] Elastomeric composites have low thermal conductivity and high mechanical strength to weight ratio.[5] Ethylene propylene diene monomer rubber (EPDM) and acrylonitrile butadiene rubber (NBR) are used as elastomeric matrixes to develop ablative composites as they have excellent thermal resistance properties, appropriate mechanical strength, and easy processing.[6–8] But these matrixes alone could not survive under the severe temperature and speed conditions. Therefore, chopped/woven fibers (ceramic, Kevlar, carbon, glass, etc) and fillers (metal oxides, silica, carbon nanotubes, clays, etc) are used as reinforcements in the elastomeric polymers to enhance their thermal, mechanical, and ablation properties.[9–11] A polymer matrix ablative composite restricts the incoming heat flux through the endothermic heat quenching phenomena that are taken place during the ultrahigh temperature shear flow of hot stream of gases encountered by a space vehicle during its reentry as depicted in Figure 1.[12,13] The schematic illustration of ablation mechanism simulates that the incoming heat flux (IHF) is exposed on the surface of the ablator aligned on an aerodynamic surface and as a result the composite material starts to deplete. An ablator is divided into eroded, ablated, pyrolysis, and virgin materials zones during ablation. IHF encountered by an ablator is absorbed, reflected back, blocked, and dissipated through the transpiration, vaporization, reradiational, endothermic chemical reactions, and charring heat fluxes. Only conductive heat flux (Q_s) conducts through the ablative composite that is sensed at its backface.[14]

In the present investigation, novel NBR/ceramic fiber composites were fabricated to scrutinize the effect of variant fiber concentrations on the ablation, thermal stability/transport, and mechanical properties of polymer composites.

EXPERIMENTAL

Materials

Acrylonitrile butadiene rubber (Kumho KNB 35L, ACN content range from 34%) was purchased from ABF International Corporation limited, Korea. Carbon black (N330, 70 nm, 99% pure) was supplied by Hebei Daguangming Juwuba, Carbon Black Co.

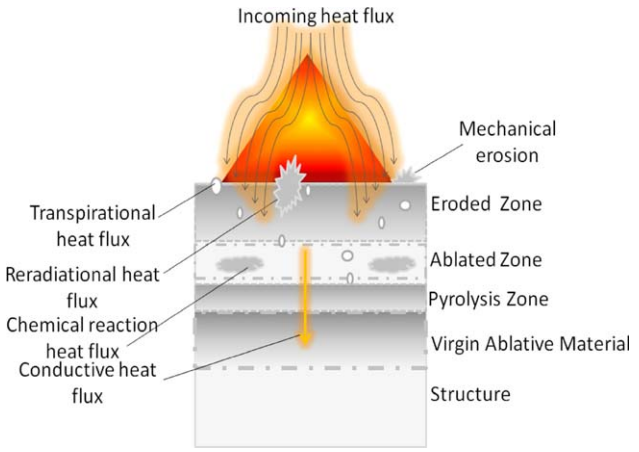

Figure 1. Schematic illustration of the ablation mechanism. [Color figure can be viewed in the online issue, which is available at wileyonlinelibrary.com.]

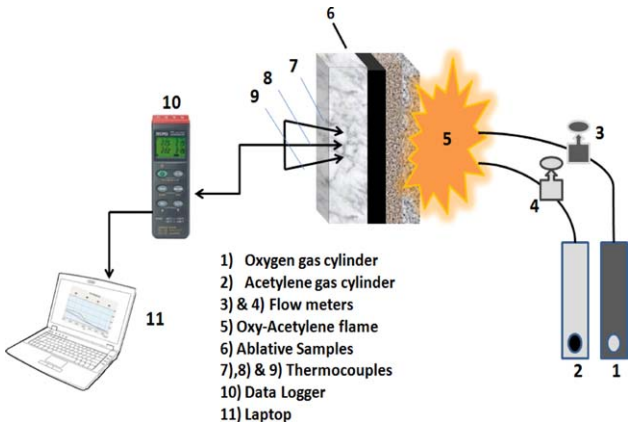

Figure 2. Experimental setup of ablation testing of the elastomeric ablative composites. [Color figure can be viewed in the online issue, which is available at wileyonlinelibrary.com.]

Sulphur, zinc oxide, and stearic acids were purchased from Merck, Germany. MBTS (Mercaptobenzthiazole disulphide) and TMTD (Tetramethylthiuram Disulfide) were received from Dalian Richon Chemical Co., China. DOP (Dioctylphathalate) and wax were supplied by International petrochemicals (Pvt) Ltd, Pakistan. Ceramic fibers ($Al_2O_3 + SiO_2$), having purity 99%, and diameter ≈2–6 μm were bought from Shandong alert soluble ceramic fiber and equipment Co., China.

Formulation of Composite Materials

Ceramic fibers (CerFs) along with the carbon black (reinforcing filler), cross linker (Sulphur), accelerators (MBTS & TMTD), activators (zinc oxide, stearic acid), and plasticizers (DOP & wax) were incorporated into the polymer matrix according to the following formulation presented in Table I.

Fabrication of Ablative and Tensile Testing Specimens

Internal dispersion kneader and two roller mixing mill were used to uniformly disperse the CerFs along with the processing aids in the NBR matrix. The preferential orientation of the incorporated fibers is along the milling direction that is parallel to the polymer matrix. So, the fibers were directed horizontally within the rubber matrix. The ablative composite specimens (NC ablators) having 0.01 m^2 area and 0.01 m thickness were fabricated on the hot isostatic press at 150°C and 11 MPa for 50 min. Four diverse concentrations of CerFs, i.e., 0, 4, 6, and 8 phr were incorporated in the rubber matrix and the fabricated composites were nominated as NC1, NC2, NC3, and NC4, respectively. Tensile testing composite specimens for all formulations were also fabricated according to the ASTM D412-98A.

Table I. Basic Formulation with Different phr Loadings of Ceramic Fibers

Sample ID/Filler (phr)	NC1	NC2	NC3	NC4
Ceramic Fiber	0	4	6	8

NBR: Nitrile butadiene rubber (100 phr)
DOP: Dioctylphatalate (7.5 phr)
MBTS: Mercaptobenzthiazole disulphide (2 phr)
TMTD: Tetramethylthiuram Disulfide (2 phr), Carbon black (40 phr)
Sulphur (2 phr), Zinc Oxide(5 phr), Streaic Acid (2 phr)

Ablation Testing

Backface Temperature Elevation and Insulation Index. Ablation testing of the NBR-CerF (NC) ablators was carried out according to the ASTM E285-08, in which Oxy-acetylene (O-A) torch was exposed on the surface of NC ablator as illustrated in Figure 2. O–A torch was used as a high temperature source (Flame temperature ≈3000°C with heat flux of 8×10^6 W/m^2 measured with pyrometer IRAH35 U, Japan) i.e. exposed on the central front facet of the NC ablator. The flow rate of both oxygen and acetylene gases was 0.35 m^3/h and their pressures were 0.344 and 0.158 MPa, respectively, during the ablation testing. The torch was kept at 10 mm far from the testing specimen surface. Backface temperature profiles of the NC ablators during the ablation testing were monitored using three thermocouples at the backface of the ablator, i.e., adhered with the aluminum tape. These temperature sensing devices were connected to the

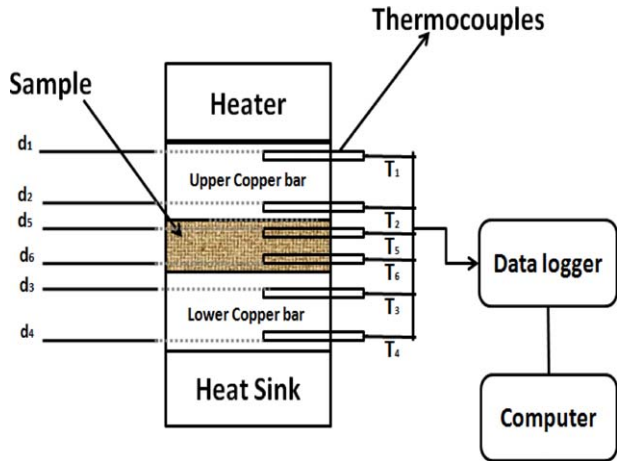

Figure 3. Designed setup for thermal conductivity/impedance measurements. [Color figure can be viewed in the online issue, which is available at wileyonlinelibrary.com.]

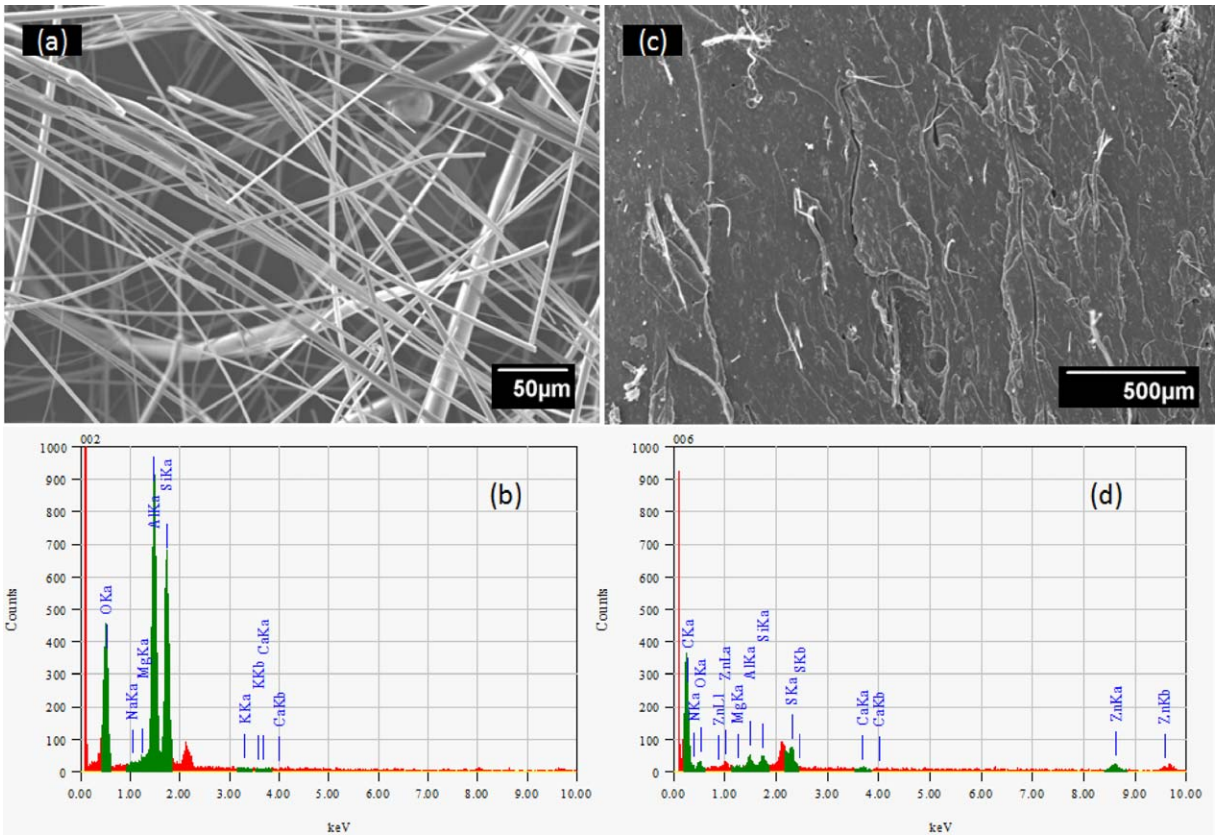

Figure 4. SEM and EDS analysis of ceramic fibers (a,b), incorporated fibers dispersion in the NBR matrix (c) and the compositional analysis of the fabricated composites (d). [Color figure can be viewed in the online issue, which is available at wileyonlinelibrary.com.]

datalogger, Tecpel 319, i.e., also linked with the laptop through RS-232 data cable. Ablation test was performed for 200 s. The ablative specimens were engraved in a ceramic tile during their ultrahigh temperature ablation investigation.

Time–temperature contours were developed meanwhile during the ablation testing of NC ablators on the laptop display. Insulation indexes (I_T) of the ablative composites were measured according to the following formulae.[15]

$$\text{Insulation Index of the NC ablator} = I_T = \frac{t_T}{d_o} \quad (1)$$

Where t_T is the time required to reach at a specific backface temperature T of the ablator having thickness d_o.

Ablation Rates and % Char Yield. Linear/mass ablation rates and % char yields of NC ablated specimens were measured using the following mathematical equations, i.e.,

$$\text{Linear ablation rate of the NC ablator} = v_l = (d_o - d_1')/t \quad (2)$$

$$\text{Mass ablation rate of the NC ablator} = v_m = (m_1 - m_2)/t \quad (3)$$

$$\%\text{char yield of the NC ablator} = C_P = \frac{(m_1 - m_2) * 100}{m_1} \quad (4)$$

Where d_o, m_1, and d_1', m_2 are the thickness and mass of the NC ablator before and after O-A flame exposure, respectively and t is the ablation testing duration.[16]

Thermophysical Properties

Thermal conductivity of the polymer nanocomposites specimens were carried out using ASTM E1225-99. Schematic illustration of comparative guarded longitudinal heat flow system in Figure 3 shows the possible locations of temperature sensors, heating source, water heat sinker, temperature data logger, and a laptop. Time–temperature contours of all thermocouples located at specific positions were displayed on the laptop screen via OQ610 Portable Temperature Data Logger. Thermal conductivity of the composite specimens was measured using eq. (5).[17,18]

$$\text{Thermal conductivity of testing composite} = \kappa_s = \frac{(q_T' + q_B')(d_4 - d_3)}{2(T_4 - T_3)} \quad (5)$$

where

$$\text{Heat flow at top bar} = q_T' = \kappa_M \left(\frac{T_2 - T_1}{d_2 - d_1}\right)$$

$$\text{Heat flow at bottombar} = q_B' = \kappa_M \left(\frac{T_6 - T_5}{d_6 - d_5}\right)$$

where κ_M = Thermal conductivity of the copper bar, T_1, T_2, T_3, T_4, T_5, and T_6 are the temperatures of six thermocouples in °C and d_1, d_2, d_3, d_4, d_5, and d_6 are their corresponding positions.

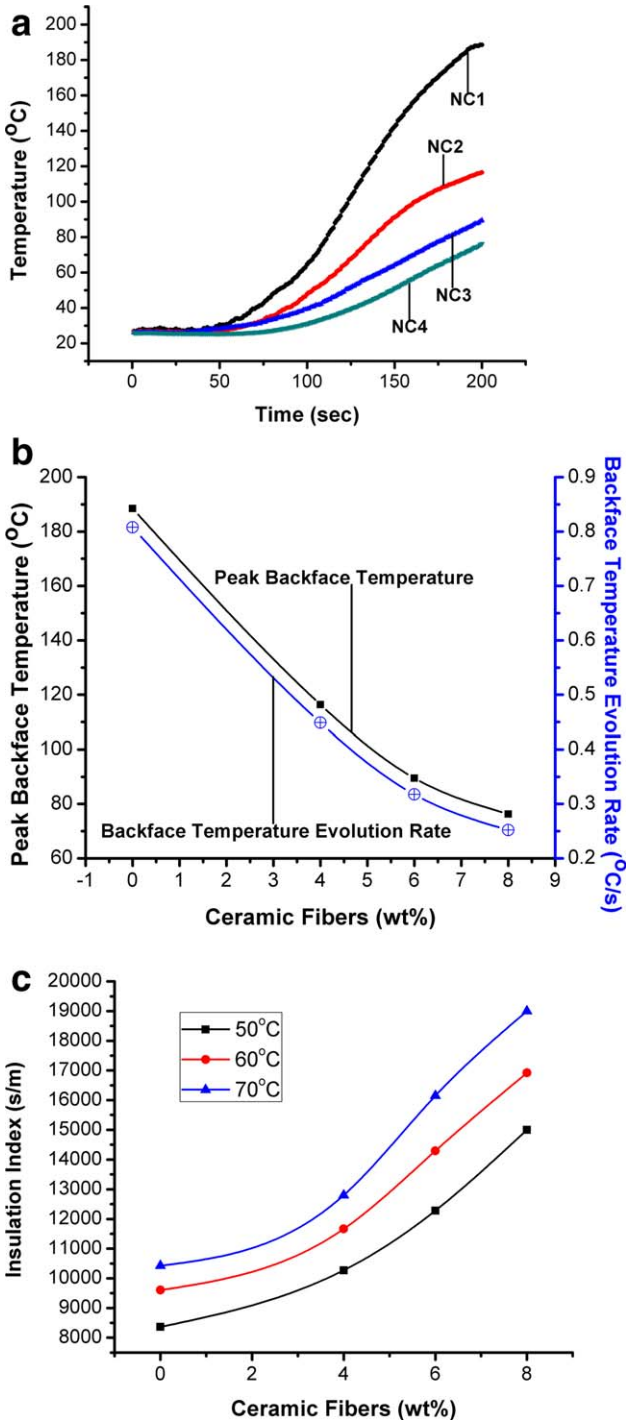

Figure 5. (a) Backface time–temperature contours of the ceramic fibers impregnated NBR composites. (b) Peak backface temperature and temperature evolution rate at backface of ablative composites at different CerFs concentrations. (c) Insulation indexes at diverse ceramic fiber loadings in the rubber matrix. [Color figure can be viewed in the online issue, which is available at wileyonlinelibrary.com.]

Thermal impedance of a material is its ability to resist thermal/temperature fluctuations in a variable heating environment. For thermal impedance, four thermocouples have been used instead of six in afore mentioned thermal conductivity apparatus. Thermal impedance of the nanocomposite specimens were measured according to ASTM D5470-01 and by following eq. (6).

$$\text{Thermal impedance } \left(m^2 * K/W\right) = I = \left(\frac{\kappa_P * A}{F}\right)(T_A - T_D)$$

Where F = Heat Input (W) = Electrical potential (V) × Electrical current (I)

Temperature of upper bar in contact with testing composite

$$(^{\circ}\text{C}) = T_A = T_2 - (T_1 - T_2)\left(\frac{d_B}{d_A}\right)$$

Temperature of lower bar in contact with testing composite

$$(^{\circ}\text{C}) = T_D = T_3 - \left(T_3 - T_4\right)\left(\frac{d_D}{d_C}\right)$$

where T_1 (°C) = Upper temperature of upper bar, T_2 (°C) = lower temperature of upper bar, T_3 (°C) = Upper temperature of lower bar, T_4 (°C) = Lower temperature of lower bar, d_A (m) = Distance between T_1 and T_2, d_B (m) = Distance between T_2 and testing composite, d_C (m) = Distance between T_3 and T_4, and d_D (m) = Distance between testing composite and T_3.

Thermal Degradation

Thermal stability and endothermic/exothermic behavior of these composites were analyzed through Perkin Elmer Diamond TG/DTA, Japan. Heating rate and temperature range during the thermogravimetric study of the polymer composite specimens was 10°C/min and 25–1000°C, respectively.

Mechanical Properties

Ultimate tensile testing machine (UTM, 20KNXD Plus, Shimadzu) was used to evaluate ultimate tensile strength, elongation at break, and modulus of elasticity of the tensile testing specimens according to the ASTM D418-98A. Shore A rubber hardness of the composite specimens were appraised using Torsee, Tokyo testing machine.

Morphological Characterization

Scanning electron microscopy (SEM, JSM 6940A, Jeol, Japan) along with the energy dispersive X-ray spectroscopy (EDS) were used for spectroscopic and compositional analyses of the tensile fractured specimens, ablated composite samples, and CerFs.

RESULTS AND DISCUSSION

CerFs Dispersion in the Rubber Matrix

Aluminum silicate fibers having average diameter 2.7 μm are depicted in Figure 4(a) along with the CerF's EDS analysis in Figure 4(b) that illustrates the presence of three major elements Al, Si, and O. The even distribution of CerFs in the rubber matrix is achieved due to the longitudinal and transverse flow of material through the twin roll nip of heated two roller mixing mill. Well dispersed CerFs in the NBR matrix are observed in Figure 4(c) coupled with the elemental analysis that simulates the existence of N, C, O, Si, Al, Zn, and S in the NC4 ablator in Figure 4(d). The presence of Al and Si elements in the

Applied Polymer SCIENCE

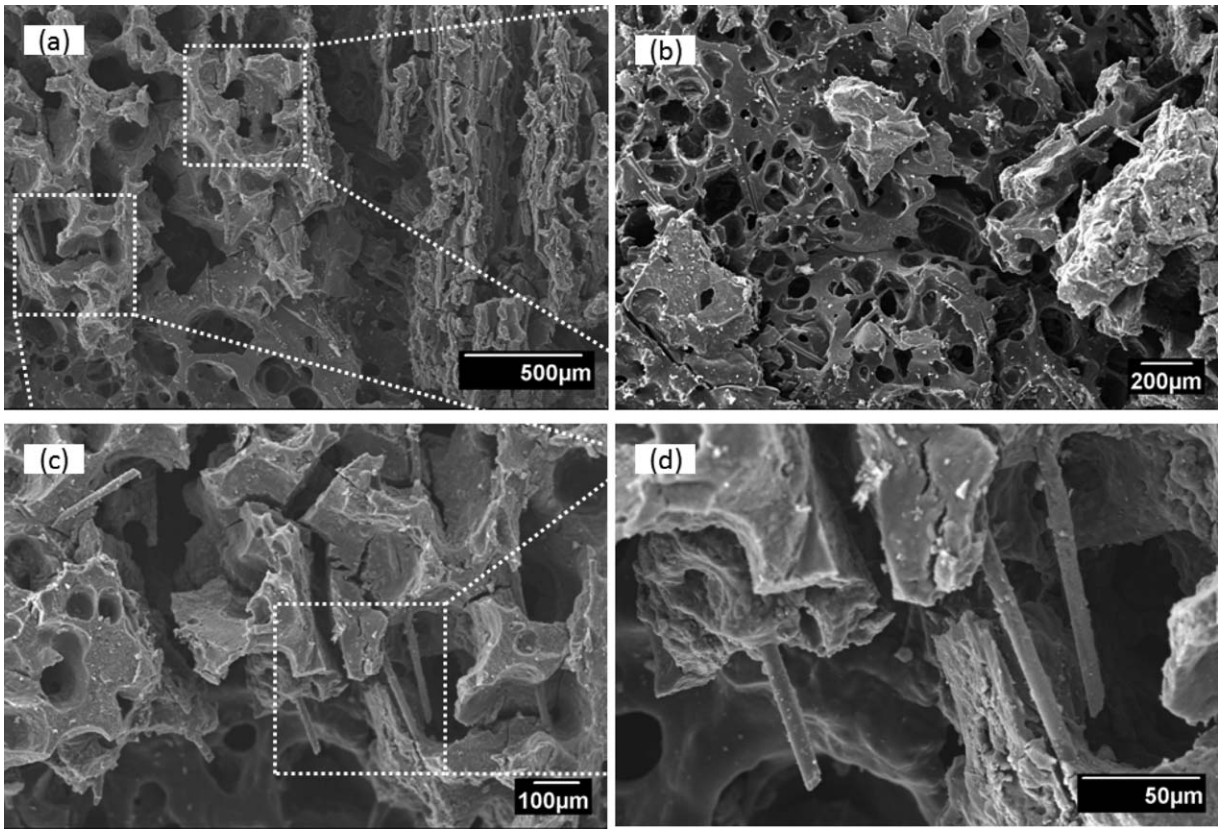

Figure 6. (a–d) Voids formation during ablation, polymer pyrolysis, char reinforcement interaction, and distributed ceramic fibers in the NC4 ablated specimen.

polymer composite EDS analysis also confirms the well distribution of ceramic fibers within the polymer matrix.

Backface Temperature Evolution and Insulation Index

Backface temperature evolution (BTE) of the NC ablators during the ablation testing is portrayed in Figure 5(a). Time–temperature contours of the ablative composites illustrates that BTE is diminished with increasing CerFs concentration in the rubber matrix. The maximum backface temperatures after 200 s O–A flame exposure on the facets of NC ablators are observed 188.90, 117.22, 89.81, and 76.06°C for NC1, NC2, NC3, and NC4, respectively, as clear from Figure 5(b). It means that the incorporation of 8 phr CerFs in the polymer matrix reduces the peak backface temperature up to 112°C compared to NC1 ablator due to the low thermal conductivity/diffusivity and high thermal stability of the aluminum silicate fibers.[19,20] Backface

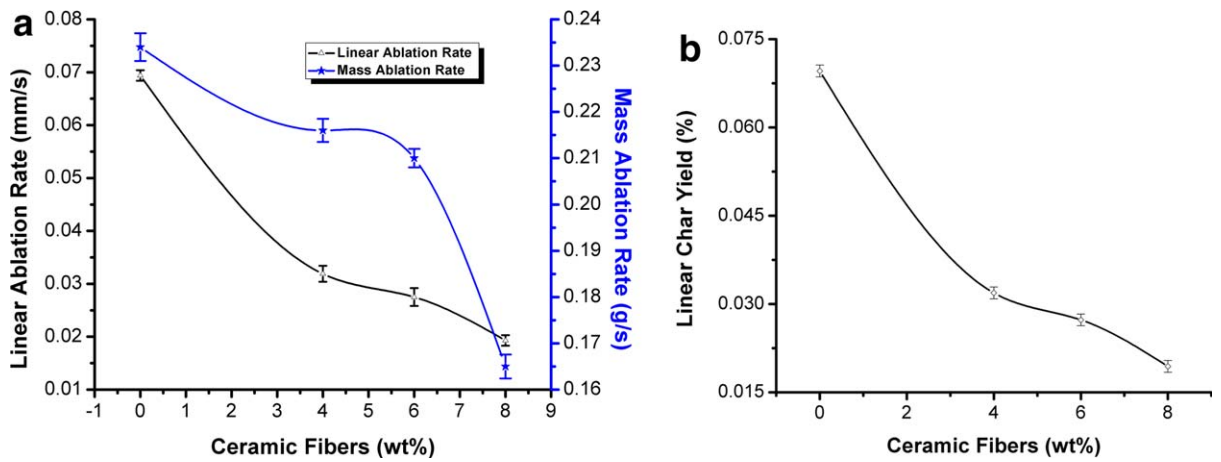

Figure 7. (a) Linear/mass ablation rates of the ablative composites at different CerFs concentrations in the polymer matrix. (b) % char yield contours of the ablative composites at different CerFs concentrations in the polymer matrix. [Color figure can be viewed in the online issue, which is available at wileyonlinelibrary.com.]

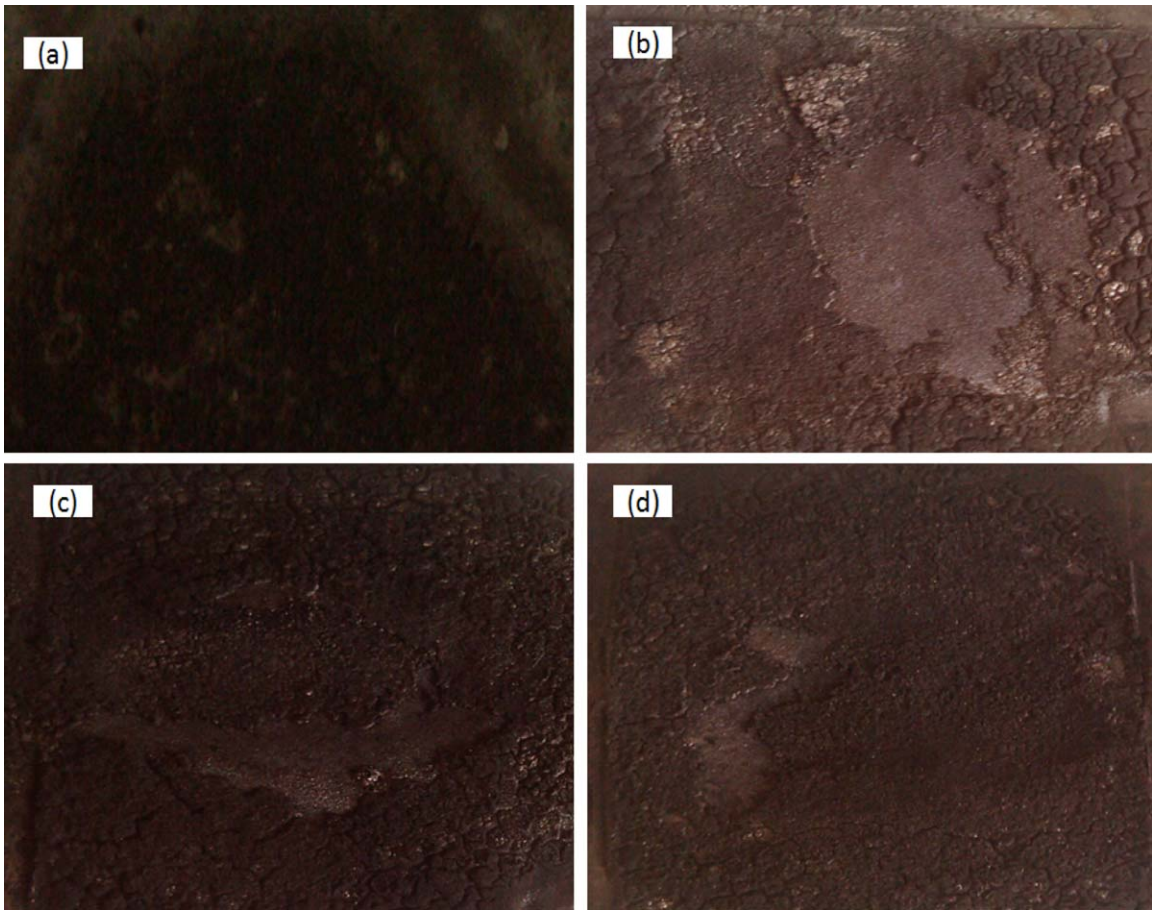

Figure 8. Post burnt ablative composites (a) NC1 ablator, (b) NC2 ablator, (c) NC3 ablator, and (d) NC4 ablator. [Color figure can be viewed in the online issue, which is available at wileyonlinelibrary.com.]

temperature evolution rates (BTER) of the NC ablators are also displayed in Figure 5(b) that shows the decline of BTER from 0.8 to 0.25°C/s with increasing fiber concentration from 0 to 8 phr in the rubber matrix. Insulation indexes (I_T) of the composite specimens at backface temperatures 50, 60, and 70°C were measured according to the eq. (1) and depicted in Figure 5(c). A remarkable I_T enhancement at all selected temperatures is observed with increasing fiber concentration in the rubber matrix. So, NC4 can withstand against high temperature gases flow for a prolonged duration compared to the NC1 ablator, counterpart. SEM micrographs of the ablated NC4 composite specimen at diverse magnifications are depicted in Figure 6. A portion of the front surface of the ablated specimens during the linear ablation test of NC4 (8 phr loaded NBR composite), was analyzed for microscopic analysis. Well dispersed microfibers, porous char, and char reinforcement interaction are observed in these micrographs. The porous structure of the ablated sample enhances the transpiration and vaporization heat fluxes, which reduce the backface temperature elevation during the ablation testing of the composite specimens.[21]

Ablation Resistance and % Char Yield

Linear and mass ablation rates of the ablated composite specimens were measured using eqs. (2) and (3) and displayed in Figure 7(a). Linear/mass ablation resistance augmentation according to the descending order NC4 < NC3 < NC2 < NC1 is observed in the ablation rates contours. The least linear and mass ablation rates are measured for NC4 ablator, i.e., 0.02 mm/s and 0.165 g/s. It means that CerFs incorporation in the rubber matrix has remarkably enhanced the ablation resistance of the fabricated composite specimens. Percent char yields of the eroded ablators are measured using eq. (4) and the effect of CerFs concentration on the % char yield of the composite specimens is depicted in Figure 7(b). Similar to ablation resistance, % char yield is also diminished with increasing fiber impregnation in the host polymer matrix due to the high thermal stability of CerFs. The photographs of the NC1, NC2, NC3, and NC4 ablated specimens are portrayed in Figure 8(a–d) respectively. Due to the appropriate interaction between the ablated zone and virgin material zone is observed that eventually promotes the mechanical erosion resistance of the ablative composites, i.e., a key parameter in hyperthermal and hypersonic environments encountered by an aerodynamic surface during its mission.

The role of ceramic fibers to enhance the ablation resistance of the fabricated ablative composites is owing to the excellent thermal stability of the impregnated fibers, development of the strong ablated char layer due to the interaction between the melted fibers, and the charred polymer, i.e., char-reinforcement interaction during the ablation test. The melting of

Applied Polymer SCIENCE

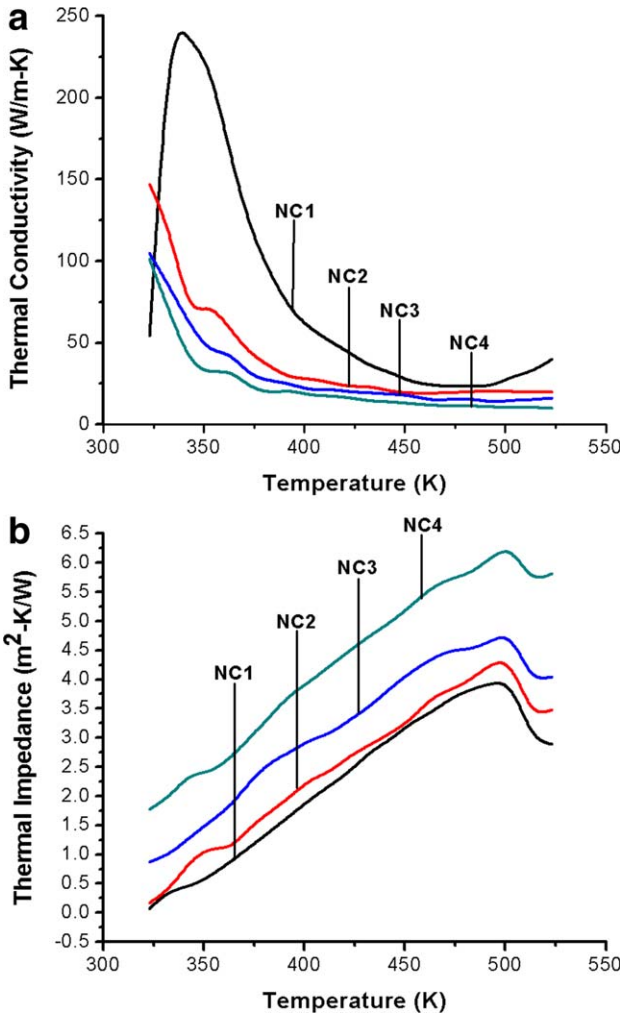

Figure 9. (a) Thermal conductivity of the CerFs impregnated NBR composites in the temperature span 323K–523K. (b) Thermal impedance of the CerFs incorporated NBR composites in the temperature span 323K–523K. [Color figure can be viewed in the online issue, which is available at wileyonlinelibrary.com.]

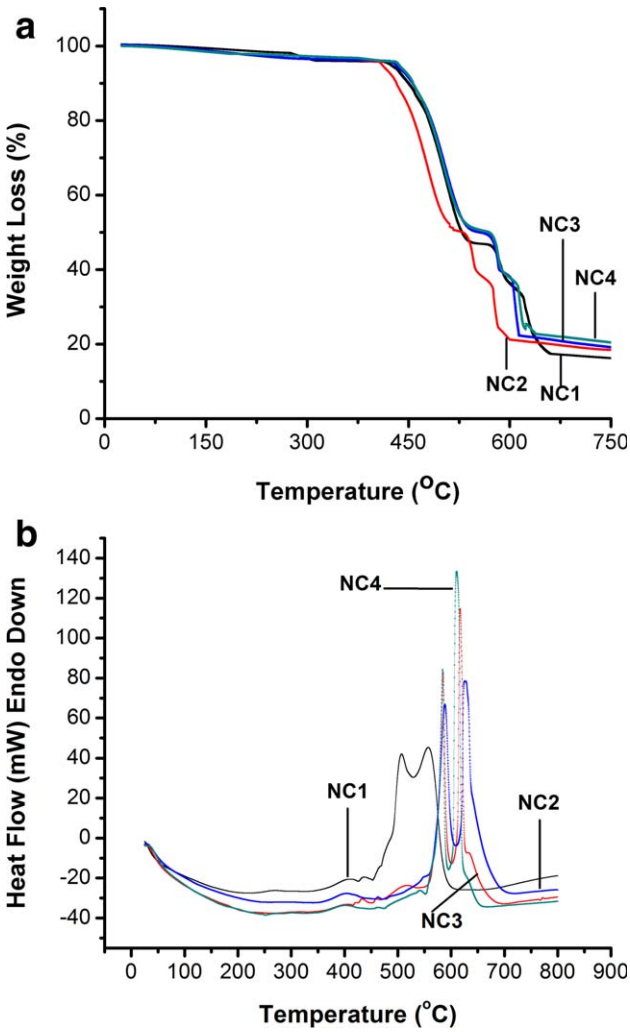

Figure 10. (a) The effect of ceramic fiber concentration on the thermal degradation of the NC composites. (b) The effect of ceramic fiber concentration on the heat flow response of NC composites. [Color figure can be viewed in the online issue, which is available at wileyonlinelibrary.com.]

"$Al_2O_3 + SiO_2$" fibers is taken place from 1400 to 1800°C and these fibers absorb enormous heat during melting. Additionally, in this temperature range, char-reinforcement reactions are occurred that results in the formation of Al_4C_3 and SiC layer that efficiently protects the composite during the impingement of oxy-acetylene torch flame on the surface of the ablator.[22]

Thermal Conductivity/Impedance

Thermal conductivity (TC) of the micro-ceramic fibers impregnated rubber composite specimens was measured in the temperature span 323–523 K according to ASTM E1225-99 and eq. (1). The accumulated data are presented in the Figure 9(a). TC of the composite specimens was reduced with increasing the testing temperature due to the activation of endothermic heat quenching phenomena that were taken place within the polymer composite. The heat absorbed by the composite specimens to overcome the molecular bond strength of the polymeric chains and transpirational/vaporizational cooling effects are the possible facts that limit the thermal conduction through the polymer composite. The uniform and successful incorporation of CerFs into the rubber matrix has efficiently diminished the TC of the fabricated composite formulations owing to the excellent thermal stability and endothermic capability of the impregnated fibers. The utmost TC is observed for NC1 (43.54 W/m-K) whereas minimum is noticed for NC4 (16.19 W/m-K) at 423 K.[23,24]

Table II. Mass Loss (%) of NC Composites at Different Temperatures

Sample ID	Mass loss (%) at 300°C	Mass loss (%) at 500°C	Mass loss (%) at 600°C	Mass loss (%) at 700°C
NC1	3.58	30.98	63.72	82.65
NC2	3.58	45.24	77.45	80.18
NC3	3.3	28.82	62.29	78.89
NC4	2.45	30.5	61.99	77.59

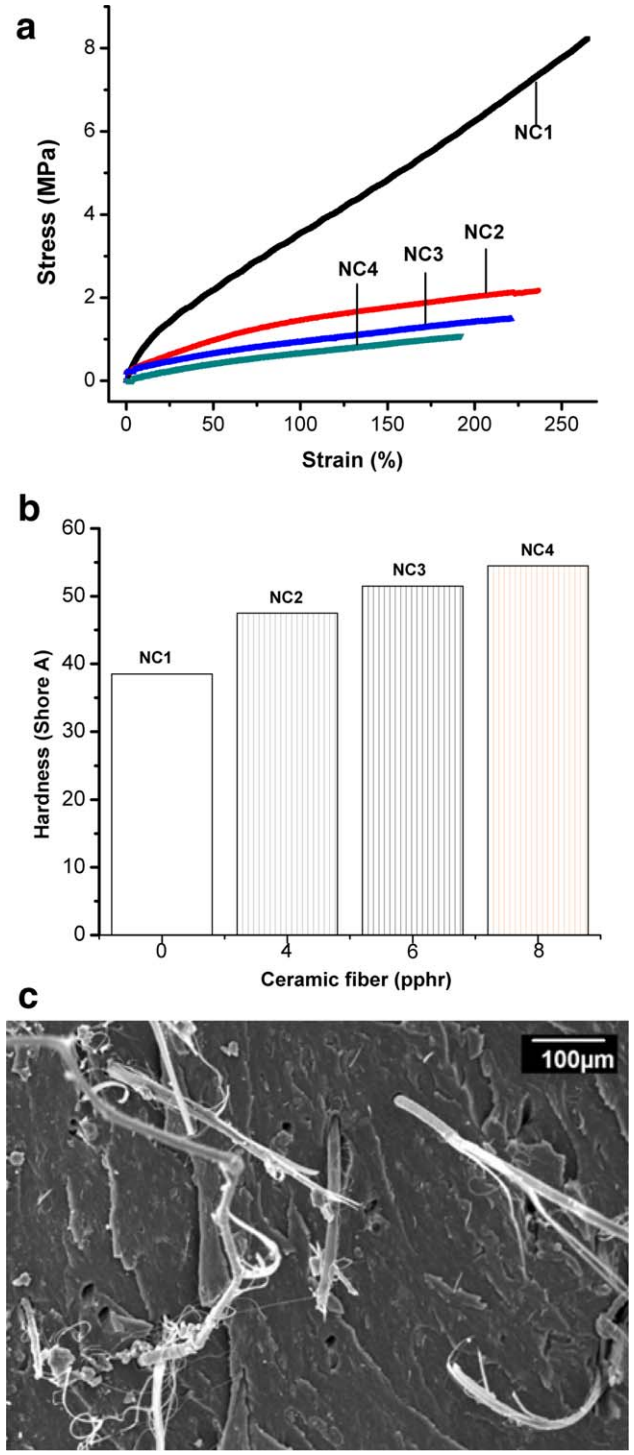

Figure 11. (a) Stress–Strain contours of the NC composites. (b) Variation in shore A hardness of the composite specimens with diverse loadings of ceramic fibers in the rubber matrix. (c) SEM image of NC4 fractured sample in tensile mode. [Color figure can be viewed in the online issue, which is available at wileyonlinelibrary.com.]

Thermal impedance (TI) of the composite specimen was measured using eq. (6) and ASTM D5470-03 in Figure 9(b). TI is an important thermal characteristic which tells the capability of a material to resist thermal gradient atmosphere. TI of the polymer composite specimens is enhanced with increasing temperature up to 500 K and then a decline is observed in the proceeding temperature span due to the elevation in atomic vibrational acceleration which maximizes the phonon transport and as a result reduces the thermal resistance of the tested composite specimen. The utmost impregnation of CerFs in the rubber matrix has augmented the TI of the composite specimen up to 86% compared to the base composite formulation (NC1) due to the remarkable thermal endurance and heat quenching ability of the incorporated CerFs.[25,26]

Table III. Mechanical Properties of NC Composites

Sample ID	Ultimate tensile strength (MPa)	Elongation at break (%)	100% Modulus (MPa)
NC1	8.19	264.70	3.53
NC2	2.17	236.43	1.47
NC3	1.50	220.23	0.92
NC4	1.09	191.96	0.65

Thermal Stability

Thermogravimetric analysis in Figure 10(a) and Table II illustrate the thermal stability enhancement with the progressive addition of CerFs in the rubber matrix due to their high thermal stability and low thermal conductivity. The maximum mass loss in the heating air environment for all ablators is observed in the temperature range 500–650°C. The mass loss measurements at 300, 500, 600, and 700°C show that NC4 has the maximum capability to withstand against the heat flow as clear from Table II. Differential thermal analysis in Figure 10(b) of the composite specimens also reveals the effective heat absorbance evolution with increasing the concentration of CerFs in the host polymer matrix and NC4 absorbs maximum input heat.[27] The maximum heat variation regarding heat absorbance and exhaust is observed in the polymer composites pyrolysis temperature range.[28,29]

Mechanical Properties

Stress–strain curves, tensile strength, elongation at break, 100% modulus, and Shore A hardness are depicted in Figure 11(a,b) and Table III. The incorporation of CerFs in the NBR matrix has inversely affected the mechanical properties, while Shore A hardness of the NC ablators has been augmented up to 42%. Ceramic fibers have low tensile strength, elongation at break, and bending modulus as compared to polymeric synthetic fibers (Kevlar, Spectra fibers, etc), but they have excellent thermal endurance and insulation characteristics. The tensile fracture of the composite specimen also elaborate the matrix–filler debonding and CerF's pull out due to weak fiber–matrix bond as clear in Figure 11(c).[30–32]

CONCLUSION

Microsize ceramic fibers have been uniformly dispersed in the NBR matrix using two roller mixing mill. The peak backface temperatures at the back facet of the NCL ablators are

diminished from 190°C (NC1) to 80°C (NC4) with increasing fiber concentration in the rubber matrix. Linear/mass ablation rates, insulation index and % char yield data of the NC ablators illustrate the incredible enhancement in anti-ablation performance with the progressive incorporation of CerFs in the polymer matrix. Aluminum silicate fibers have progressively influenced the thermal stability and heat absorbance capability of the fabricated ablators. Thermal conductivity is reduced down to 63% while thermal impedance of the composite specimens is augmented up to 86% with the utmost CerFs impregnation in the base composite formulation (NC1). Tensile properties of the ablative composites are degraded while the rubber hardness is augmented with increasing CerFs concentration in the host matrix.

ACKNOWLEDGEMENT

The authors would like to greatly acknowledge Longman mills, Lahore and Pakistan Railway Carriage Factory, Islamabad for providing facilities regarding fabrication and Ablation testing of the NC ablative composites.

REFERENCES

1. Park, J. K.; Cho, D.; Kang, T. J. *Carbon* **2004**, *42*, 795.
2. Lin, W. S.; *Int. J. Heat Mass Trans.* **2005**, *48*, 5504.
3. Srebrenkoska, V.; Bogoeva-Gaceva, G.; Dimeski, D. *J. Serb. Chem. Soc.* **2009**, *74*, 441.
4. Soo Kim, E.; Lee, T. H.; Shin, S. H.; Yoon, J. S. *J. Appl. Polym. Sci.* **2011**, *120*, 831.
5. Venkatapathy, E.; Arnold, J.; Laub, B.; Hartman, G. *Adv Space Res* **2009**, *44*, 138.
6. Kang, T. J.; Shin, S. J.; Jung, K.; Park, J. K. *Carbon* **2006**, *44*, 833.
7. Gao, G.; Zhang, Z.; Li, X.; Meng, Q.; Zheng, Y. *Polym. Bull.* **2009**, *64*, 607.
8. Park, J. K.; Kang, T. *J. Carbon* **2002**, *40*, 2125.
9. Galledari, N. A.; Beheshty, M. H.; Barmar, M. *J. Appl. Polym. Sci.* **2011**, 1597.
10. Gao, G.; Zhang, Z.; Li, X.; Meng, Q.; Zheng, Y.; Jin, Z. *J. Appl. Polym. Sci.* **2010**, *118*, 266.
11. Qiu, J.; Cao, X.; Tian, C.; Zhang, J. *J. Mater.Sci.Technol.* **2005**, 21.
12. Iqbal, N.; Sagar, S.; Khan, M. B.; Rafique, H. M. *Polym. Eng. Sci.* **2013**.
13. Iqbal, N.; Sagar, S.; Khan, M. B.; Rafique, H. M. *J. Compos. Mater.* **2013**.
14. Al-Safy, R.; Al-Mahaidi, R.; Simon, G. P.; Habsuda, J. *Construct. Build. Mater.* **2012**, *28*, 769.
15. Iqbal, N.; Khan, M. B.; Sagar, S.; Maqsood, A. *J. Appl. Polym. Sci.* **2013**, *128*, 2439.
16. Pulci, G.; Tirillŋ, J.; Marra, F.; Fossati, F.; Bartuli, C.; Valente, T. *Compos. Part A-Appl. Sci.* **2010**, *41*, 1483.
17. Pham, D. C. *Int. J. Heat Mass Trans.* **2008**, *51*, 3355.
18. Yau, Y. H.; Wong, H. F.; Ahmad, N. *Int. J. Heat Mass Trans.* **2012**, *55*, 2879.
19. Bahramian, A. R.; Kokabi, M. *J. Hazard. Mater.* **2008**, *166*, 445.
20. Lombardi, M.; Fino, P.; Malucelli, G.; Montanaro, L. *Compos. Struct.* **2011**, *94*, 1067.
21. Bahramian, A. R.; Kokabi, M.; Famili, M. H. N.; Beheshty, M. H. *J. Hazard. Mater.* **2008**, *150*, 136.
22. Torre, L.; Kenny, J.; Boghetich, G.; Maffezzoli, A. *J. Mater. Sci.* **2000**, *35*, 4563.
23. Mu, L. W.; Shi, Y. J.; Feng, X.; Zhu, J. H.; Lu, X. H. *Tribol. Int.* **2012**, *53*, 45.
24. Maqsood, A.; Anis-ur-Rehman, M.; Kamran, K.; Gul, I. H. *J. Phys. D: Appl. Phys.* **2004**, *37*, 1845.
25. Yu, H.; Li, L. L.; Kido, T.; Xi, G. N.; Xu, G. C.; Guo, F. *J. Appl. Polym. Sci.* **2011**, *124*, 669.
26. Sagar, S.; Iqbal, N.; Maqsood, A. *J. Reinf. Plast. Compos.* **2013**.
27. Rathinasamy, P.; Balamurugan, P.; Balu, S.; Subrahmanian, V. *J. Appl. Polym. Sci.* **2003**, *91*, 1111.
28. Arrieta, C.; David, E.; Dolez, P.; Vu-Khanh, T. *J. Appl. Polym. Sci.* **2009**, *115*, 3031.
29. Sagar, S.; Iqbal, N.; Maqsood, A.; Javaid, U. *J. Therm. Anal. Calorim.*, 1.
30. Sarkhel, G.; Choudhury, A. *J. Appl. Polym. Sci.* **2008**, *108*, 3442.
31. Pysher, D. J.; Goretta, K. C.; Hodder Jr., R. S.; Tressler, R. E. *J. Am. Ceram. Soc.* **1989**, *72*, 284.
32. Hlavacek, V.; Revankar, V. V. S. A Collection of Papers Presented at the 13th Annual Conference on Composites and Advanced Ceramic Materials, Part 1 of 2: Ceramic Engineering and Science Proceedings, Volume 10, Issue 7/8, **2008**, pp 911.